The Astronomical Journal, 155:227 (5pp), 2018 June https://doi.org/10.3847/1538-3881/aabc5a

A Search for Molecular Gas in the Host Galaxy of FRB 121102

Geoffrey C. Bower[1], Ramprasad Rao[1], Melanie Krips[2], Natasha Maddox[3], Cees Bassa[3], Elizabeth A. K. Adams[3,4], C. J. Law[5], Shriharsh P. Tendulkar[6], Huib Jan van Langevelde[7,8], Zsolt Paragi[7], Bryan J. Butler[9], and Shami Chatterjee[10]
[1] Academia Sinica Institute of Astronomy and Astrophysics, 645 N. A'ohoku Place, Hilo, HI 96720, USA; gbower@asiaa.sinica.edu.tw
[2] Institut de Radioastronomie Millimetrique (IRAM), Domaine Universitaire, 300 rue de la Piscine, F-38406 Saint-Martin-d'Hres, France
[3] ASTRON, The Netherlands Institute for Radio Astronomy, Postbus 2, 7990 AA, Dwingeloo, The Netherlands
[4] Kapteyn Astronomical Institute, University of Groningen, Postbus 800, 9700 AV, Groningen, The Netherlands
[5] Department of Astronomy and Radio Astronomy Lab, University of California, Berkeley, CA 94720, USA
[6] Department of Physics, McGill University, 3600 University Street, Montreal, QC H3A 2T8, Canada
[7] Joint Institute for VLBI ERIC, Postbus 2, 7990 AA Dwingeloo, The Netherlands
[8] Sterrewacht Leiden, Leiden University, Postbus 9513, 2300 RA Leiden, The Netherlands
[9] National Radio Astronomy Observatory, Socorro, NM 87801, USA
[10] Cornell Center for Astrophysics and Planetary Science and Department of Astronomy, Cornell University, Ithaca, NY 14853, USA
Received 2017 September 18; revised 2018 April 2; accepted 2018 April 4; published 2018 May 11

Abstract

We present Submillimeter Array and Northern Extended Millimeter Array observations of the host galaxy of FRB 121102 in the CO 3–2 and 1–0 transitions, respectively. We do not detect emission from either transition. We set 3σ upper limits to the CO luminosity $L_{\rm CO} < 2.5 \times 10^7\,{\rm K\,km\,s^{-1}\,pc^{-2}}$ for CO 3–2 and $L_{\rm CO} < 2.3 \times 10^9\,{\rm K\,km\,s^{-1}\,pc^{-2}}$ for CO 1–0. For Milky Way–like star formation properties, we set a 3σ upper limit on the H_2 mass of $2.5 \times 10^8\,M_\odot$, slightly less than the predictions for the H_2 mass based on the star formation rate. The true constraint on the H_2 mass may be significantly higher, however, because of the reduction in CO luminosity that is common for low-metallicity dwarf galaxies like the FRB host galaxy. These results demonstrate the challenge of identifying the nature of FRB progenitors through study of the host galaxy molecular gas. We also place a limit of 42 μJy (3σ) on the continuum flux density of the persistent radio source at 97 GHz, consistent with a power-law extrapolation of the low-frequency spectrum, which may arise from an active galactic nucleus or other nonthermal source.

Key words: galaxies: dwarf – galaxies: star formation – ISM: molecules – radio lines: galaxies – stars: black holes – stars: neutron

1. Introduction

Fast radio bursts (FRBs) are millisecond-duration, highly dispersed radio transients (Lorimer et al. 2007; Thornton et al. 2013). Approximately 30 FRBs have been identified in the past decade (Petroff et al. 2016). The large dispersion measure (DM) of FRBs suggests that they are of extragalactic origin, implying radio luminosities significantly in excess of any known phenomenon. A wide variety of models have been proposed (e.g., Falcke & Rezzolla 2014; Loeb et al. 2014; Connor et al. 2016; Lyutikov et al. 2016; Kashiyama & Murase 2017). These include neutron star progenitors, primarily due to the observational similarity between pulsar and FRB properties. Other models include stellar and supermassive black holes along with more exotic high-energy phenomena such as cosmic strings (e.g., Cai et al. 2012).

Of the known FRBs, all but one have been observed to produce only a single pulse in spite of tens to hundreds of hours of follow-up (Law et al. 2015; Petroff et al. 2015). FRB 121102, on the other hand, has now been detected more than 100 times (Spitler et al. 2014; Gajjar et al. 2018). This repetition has enabled targeted observing campaigns to localize FRB 121102 to an accuracy better than 100 mas using the Very Large Array (Chatterjee et al. 2017; Law et al. 2017) and better than 10 mas using the European Very Long Baseline Interferometry (VLBI) Network (Marcote et al. 2017). The FRB is spatially coincident with a compact ($\lesssim$1 mas), persistent radio source that may be associated with an accreting supermassive black hole, a supernova remnant (SNR), or a pulsar wind nebula (PWN), although each of these identifications is problematic for different reasons. In particular, the persistent radio source is orders of magnitude more luminous than any known SNR or PWN, making that explanation difficult. On the other hand, while the radio luminosity and upper limit on the X-ray luminosity are consistent with an active galactic nucleus (AGN), there is only one known example of a radio luminous AGN in a dwarf galaxy (Henize 2-10; Reines et al. 2011) despite extensive searches (e.g., Reines et al. 2013; Ofek 2017). Further, as noted below, there is no evidence of AGN activity in the FRB host galaxy based on optical spectroscopy.

The FRB is associated with a dwarf galaxy at $z = 0.19273 \pm 0.00008$, $<10^8\,M_\odot$ in stellar mass, and diameter $\approx 2''$ ($\sim$3 kpc; Bassa et al. 2017; Kokubo et al. 2017; Tendulkar et al. 2017). High-resolution imaging with the *Hubble Space Telescope* shows a bright, compact (80 mas) knot of continuum emission coincident with the FRB and the persistent radio source, along with diffuse, extended emission.

Analysis of emission lines in the optical spectrum shows evidence of star formation with an SFR $\approx 0.2\,M_\odot\,{\rm yr^{-1}}$ and no evidence for an AGN. Spectral analysis places a constraint on the metallicity of $\log_{10}[{\rm O/H}]+12 \approx 8.0$ (Kobulnicky & Kewley 2004; Bassa et al. 2017), indicating significantly subsolar metallicity, which is common for dwarf galaxies. Low-metallicity dwarf galaxies have been identified as hosts to long gamma-ray bursts (GRBs) and superluminous supernova (Metzger et al. 2017).

Multi-wavelength studies of GRB hosts have demonstrated the power to constrain progenitor classes (e.g., Perley

et al. 2016). ALMA non-detection of carbon monoxide (CO) in two long-duration GRB hosts has shown an unusually low gas-to-dust ratio at the location of the GRB, possibly as the result of ultraviolet radiation dissociation of the CO, providing an important clue to the environment from which GRBs originate (Hatsukade et al. 2014). Further, CO spectroscopy can be an important diagnostic of molecular gas mass and dynamics in dwarf galaxies (e.g., Rubio et al. 2015). Finally, in addition to characterizing star formation in the host galaxy, CO could determine the dynamical center of the galaxy or detect the presence of an AGN through high-velocity gas (Davis et al. 2013). The CO luminosity for low-metallicity dwarf galaxies is difficult to estimate and may be significantly suppressed relative to Milky Way (MW)–like systems (Schruba et al. 2012).

In this paper, we report on Submillimeter Array (SMA) and Northern Extended Millimeter Array (NOEMA) observations of the host galaxy of FRB 121102 in CO transitions of 3–2 and 1–0. In Section 2, we describe our observations, which lead to a non-detection of CO and of the continuum emission at 97 GHz. In Section 3, we discuss the significance of those limits.

2. Observations and Results

2.1. SMA

Two observing tracks were obtained with the SMA on 2016 December 17 and 25 for a total of 11 hr on the host galaxy of FRB 121102. The array was in its compact configuration for both epochs. Atmospheric phase fluctuations were large in the first epoch and the optical depth was high, leaving only a fraction of the data usable. Weather conditions were better in the second epoch, with a typical 225 GHz opacity of 0.05. In both observations, the receiver was tuned to a frequency of 289.930 GHz, the rest frequency of the redshifted CO 3–2 transition. The SWARM correlator was configured with a 2.28 GHz bandwidth spectral window containing 1024 channels (with velocity width $\sim$2 km s^{-1}) centered on the CO 3–2 transition.

Absolute flux calibration was performed using Neptune. Bandpass calibration was performed using 3C 273 and phase calibration was performed using the compact source J0555 + 398. Standard data reduction techniques using MIR[11] and the Multichannel Image Reconstruction, Image Analysis and Display software (MIRIAD; Sault et al. 1995) were performed to flag, calibrate, and image the data. Good data from the first and second epochs were combined to create the final results. We obtained a naturally weighted image with a beam size of 2.5 × 2.0 arcsec at position angle 69°.

2.2. NOEMA

Three observing tracks were obtained with NOEMA on 2017 February 18, April 9 and 12 for a total of 9.7 hr on source. NOEMA was in its D configuration with baselines between 16 and 176 m. Receivers were tuned to 96.6 GHz for the redshifted CO 1–0 transition. The WideX correlator has a fixed configuration with 3.6 GHz wide IF bands (one per polarization) and a spectral resolution of 1.95 MHz (velocity width $\sim$6 km s^{-1}) covering the CO(1–0) frequency.

Absolute flux calibration was performed on MWC 349 or LkHa 101 and phase calibration was performed using J0555 + 398. Flagging and calibration were performed with the Grenoble Image and Line Data Analysis Software (GILDAS; Gildas Team 2013) and imaging was performed in AIPS (Greisen 2003). We obtained a naturally weighted image with a beam size of 4.1 × 3.6 arcsec at position angle 0°.

2.3. Results

We detect no line source at the position of FRB 121102 or anywhere else in the SMA and NOEMA maps. SMA maps were made with a velocity resolution of 45 km s^{-1} achieving an rms of 9 mJy. NOEMA maps were made with a velocity resolution of 38 km s^{-1} achieving an rms of 0.21 mJy. We also searched the spectra for higher-resolution features without any detection. The spectra are shown in Figure 1.

Molecular gas is typically found within a few hundred km s^{-1} of the the systemic velocity for dwarf galaxies. For example, in a sample of BCDs, Amorín et al. (2016) found CO emission within 200 km s^{-1} of the velocity of the centroid of optical emission lines. Velocity offsets and wide lines can differ by hundreds of km s^{-1} in the case of AGN and ULIRG outflows (Cicone et al. 2014). It is unlikely that such powerful outflows are present in this system: optical spectroscopy shows no evidence for either a supermassive black hole or strong starburst activity in the host galaxy. It is possible that the persistent source is the result of a low-luminosity AGN, but such systems do not drive powerful winds. The redshift uncertainty $\Delta z = 8 \times 10^{-5}$ corresponds to a velocity uncertainty of 24 km s^{-1}, less than the width of a single channel. We have searched velocities over the range −900 to +800 km s^{-1}. Thus, our search over a velocity range of 1700 km s^{-1} centered on the systemic velocity should recover any emission lines present.

We fit Gaussians with a dispersion σ of 40 km s^{-1} (FWHM $= 2\sqrt{2\log 2}\,\sigma = 94$ km s^{-1}) at the position of peak intensity in each spectrum. As discussed below, a dispersion of $\sim$40 km s^{-1} is a characteristic width likely to be found in this system. We find peak values of 10.2 ± 7.2 mJy and 0.17 ± 0.14 mJy for the SMA and NOEMA spectra, respectively, both of which are consistent with non-detections. These correspond to 3σ upper limits on the integrated line flux densities of 1430 mJy km s^{-1} and 21 mJy km s^{-1}, respectively. Since Gaussians fitted at the position of the peak intensity of a noise-like spectrum are a biased measurement, we also estimate limits biased on the rms noise in the spectra integrated over the expected line widths. We find 3σ limits of 1145 mJy km s^{-1} and 25 mJy km s^{-1}, respectively. We adopt these latter values as our upper limits for further discussion. We also fit Gaussians with an unconstrained width. These lead to low significance fits with characteristics dispersions in the range 400–600 km s^{-1} and peak intensities lower by an order of magnitude than the narrow fits; that is, essentially equivalent integrated intensity.

We can translate our upper limits on the integrated line flux density to limits on the CO luminosity (Bolatto et al. 2013). We find 3σ limits of $L_{\rm CO} < 2.3 \times 10^9$ K km s^{-1} pc^{-2} for CO 1–0 and $L_{\rm CO} < 2.5 \times 10^7$ K km s^{-1} pc^{-2} for CO 3–2.

As discussed in Bassa et al. (2017), there is weak evidence for an overdensity of sources near the FRB 121102 host galaxy that could appear through their line emission. We searched the full field of view including an IRAC galaxy 6″ southwest of the host galaxy and did not make any detection of lines at comparable sensitivity to that quoted above. In the NOEMA band, this corresponds to a redshift window 0.166 to 0.211.

[11] https://www.cfa.harvard.edu/~cqi/mircook.html

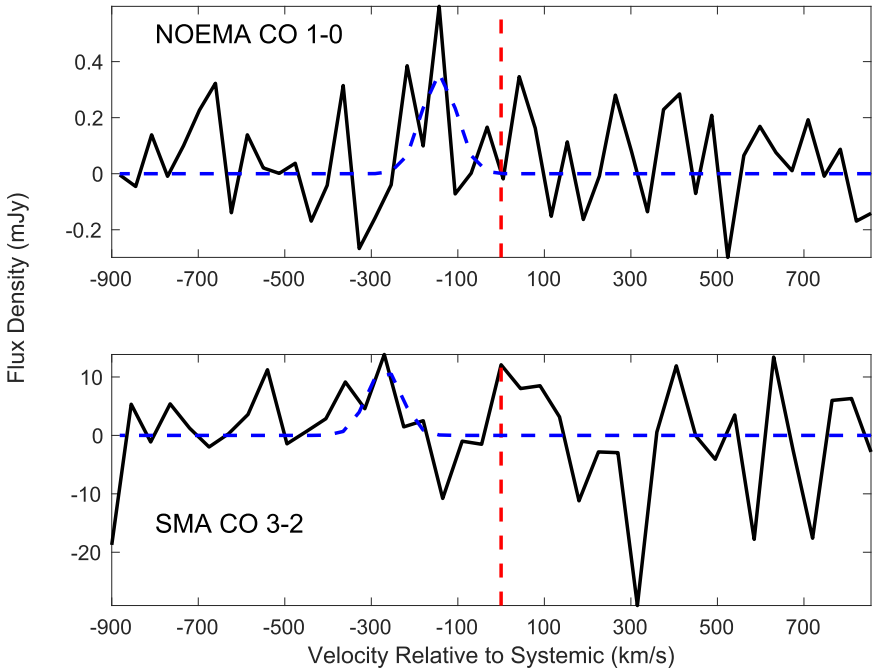

Figure 1. NOEMA CO 1–0 (top) and SMA CO 3–2 (bottom) spectra in the 1655 km s^{-1} centered on the systemic velocity. The spectra are binned into 38 and 45 km s^{-1} channels, respectively. No emission or absorption lines are present. The dashed blue lines show best-fit Gaussians with a dispersion of 40 km s^{-1} at the position of the peak intensity.

We also constructed a continuum map at 97 GHz from the NOEMA data and detected no sources in the field above a 3σ threshold of 42 μJy.

3. Discussion

In this section, we compare our luminosity limits against theoretical expectations. First, we compute an estimate of the expected H_2 mass based on observed star formation rate. This estimate along with the size of the system, lets us set a range of characteristic velocity widths for the CO line. Second, we convert our observed CO luminosity limits into an H_2 mass using MW-like conversion factors. Finally, we consider the impact of non-MW-like conversion factors on the CO luminosity and on other estimates of the H_2 mass. We also discuss the significance of the non-detection of continuum emission from the persistent radio source.

The molecular gas mass and dynamics can be estimated using standard relations derived from MW-like galaxies. Using the average star formation efficiency SFE $= 5.25 \times 10^{-10}$ yr^{-1} (Leroy et al. 2008), we can estimate the total molecular gas content from the observed FRB host SFR $= 0.23\,M_\odot$ yr^{-1} to be $M_{H_2} = 4 \times 10^8\,M_\odot$. This H_2 mass is larger than the stellar mass estimate of $\sim 10^8\,M_\odot$. Using a size of $R = 1$ kpc, we estimate a velocity dispersion $\sigma \approx \sqrt{GM_{H_2}/R} \approx 40$ km s^{-1}. We note that dark matter is often dominant in dwarf galaxies so that even in the event of lower gas or stellar mass, a velocity dispersion in the range of 40–50 km s^{-1} remains reasonable (e.g., Oh et al. 2015). This assumed line width is comparable to that seen in dwarf galaxies. For instance, Amorín et al. (2016) observed dwarf galaxy CO line dispersions in the range of 18–68 km s^{-1}.

We convert our observed CO luminosity limit into an H_2 mass limit using an MW-like conversion factor for the H_2−CO ratio $X_{CO} = 2.3 \times 10^{20}$ cm^{-2} (K km s^{-1})$^{-1}$. We use our 40 km s^{-1} limits and adopt a ratio $R_{31} = 0.5$, where R_{31} is the line ratio between the 3–2 and 1–0 transitions determined by excitation. R_{31} has an order of magnitude uncertainty. For a large sample of normal galaxies, Wilson et al. (2012) found $R_{31} = 0.18$. Schruba et al. (2012) selected the 2–1/1–0 line ratio $R_{21} = 0.7$ for their dwarf galaxy sample. We then estimate 3σ upper limits to the H_2 mass of $10^{10}\,M_\odot$ and $2.5 \times 10^8\,M_\odot$ for the 1–0 and 3–2 transitions, respectively. The latter value rejects the predicted $4 \times 10^8\,M_\odot$ mass estimate based on the SFR and the assumption of MW-like properties.

The CO luminosity may be significantly suppressed, however, relative to the expectations for an MW-like system, weakening the constraints that we have on the H_2 mass. Low metallicity has been shown to substantially reduce the CO luminosity, possibly as the result of the absence of dust shielding of UV radiation, leading to photodissociation of CO (Bolatto et al. 2013). FRB 121102 host galaxy has a metallicity $12 + \log_{10}[\mathrm{O/H}] = 8.0 \pm 0.1$, comparable to the metallicity of the Small Magellanic Cloud (SMC; Dufour et al. 1982). X_{CO} for the SMC is two orders of magnitude larger than for the MW (Schruba et al. 2012). The Large Magellanic Cloud has a metallicity higher than the SMC by $\sim$0.3 dex and a value of X_{CO} higher by a factor of 20 times the MW value (Schruba et al. 2012). Results for the Schruba et al. (2012) sample of galaxies are consistent with a power-law index $y = -2.0$ to -2.8 for $X_{CO} \propto (12 + \log_{10}[\mathrm{O/H}])^y$, depending on sample selection criteria. Amorín et al. (2016) found a value of $y = -1.5 \pm 0.3$ for their sample. Thus, predictions for the FRB 121102 host galaxy H_2 mass have an order of magnitude or more uncertainty.[12]

[12] We note that giant molecular clouds (GMCs) in theory (Wolfire et al. 2010) and in observation (Leroy et al. 2011) indicate lower values for X_{CO} than galaxy-wide measurements for low-metallicity regions. Given that our observations cover the entire galaxy, however, it is likely that the galaxy-wide conversion factors are more relevant.

The specific star formation rate and metallicity of the FRB host galaxy are typical of the population of low-mass, low-metallicity star-forming galaxies known as blue compact dwarfs (BCDs; Amorín et al. 2016). These dwarf galaxies are offset from the Schmidt–Kennicutt relation for star formation, and, thus, have shorter gas depletion timescales, or higher SFE. The SFE appropriate for the metallicity of the FRB host galaxy is much higher than that for MW-type galaxies. If we instead use this higher SFE, $\sim 3 \times 10^{-8}$, then $M_{\rm H_2} \sim 6.6 \times 10^6\,M_\odot$. Amorín et al. (2016) also find that $X_{\rm CO}$ at low metallicity is a factor of 10 larger than for MW-type galaxies. Thus, if the FRB 121102 host galaxy is representative of the BCD population, the combination of reduced H_2 mass and increased $X_{\rm CO}$ leads to one to three orders of magnitude reduction in the CO luminosity relative to the MW estimate.

Dust mass estimates also suggest that the molecular hydrogen density could be lower than estimates from the SFR. From the Hα to Hβ ratio 2.71 ± 0.26 (Kokubo et al. 2017), we estimate an upper limit on the dust mass of $\sim 10^5\,M_\odot$ (Domínguez et al. 2013). Stellar population synthesis fits to the broadband colors of the host galaxy do not require any dust contribution, leading to a similarly low estimate for the dust mass (Bassa et al. 2017). For a dust-to-gas ratio of 10^{-2}, we find an upper limit $M_{\rm H_2} < 10^7\,M_\odot$, more than an order of magnitude lower than estimated from the MW-like $X_{\rm CO}$, but consistent with the low-metallicity dwarf estimate.

Our SMA and NOEMA results show, therefore, that the FRB host galaxy is underluminous in CO relative to galaxies with MW-like star formation properties and of comparable star formation rate. An order of magnitude or more reduction in the expected CO luminosity as the result of low metallicity, however, would make the signal undetectable in either observation. Deep integrations with ALMA have the potential to detect the FRB 121102 host galaxy if its CO-to-SFR conversion is within an order of magnitude of the Milky Way.

The radio spectrum of the persistent source declines steeply at frequencies above 10 GHz and includes a 230 GHz non-detection with ALMA at a 50 μJy threshold (3σ; Chatterjee et al. 2017). An extrapolation of the low-frequency spectrum ($S \propto \nu^{-1}$) predicts a 97 GHz flux density of $\sim$20 μJy. This flux density is comparable to the $\sim 1\sigma$ threshold in the NOEMA data, and is therefore undetectable. Thus, the spectrum of the persistent source is consistent with that of an optically thin nonthermal source. AGNs and RSNe often show spectra similar to that of the persistent source (de Zotti et al. 2010). The nature of the persistent source remains ambiguous. While the spectrum is nonthermal, its luminosity significantly exceeds that of any Galactic PWNe or RSNe. An AGN interpretation of the spectrum and its luminosity is reasonable but is demographically unlikely given the rarity of radio-loud AGNs in dwarf galaxies.

The localization of FRB 121102 to a low-metallicity dwarf galaxy at cosmological distance has provided a substantial clue toward understanding the environment and nature of the host object that produces FRBs. We have searched for molecular gas emission that would serve as an important diagnostic of star formation, dynamics, and the presence of an AGN. The absence of a CO detection in our observations can be interpreted as the result of a low H_2 mass, a high CO-to-H_2 conversion factor, a high star formation efficiency, or a combination of these factors. If the host galaxy of FRB 121102 is representative of its class, then characterization of other host galaxies through molecular gas must rely on discovery of systems that differ in at least one respect: higher metallicity, greater mass, or lower redshift.

The Submillimeter Array is a joint project between the Smithsonian Astrophysical Observatory and the Academia Sinica Institute of Astronomy and Astrophysics and is funded by the Smithsonian Institution and the Academia Sinica. This work is based on observations carried out under project number E16AF001 with the IRAM NOEMA Interferometer. IRAM is supported by INSU/CNRS (France), MPG (Germany), and IGN (Spain).

Facilities: SMA, IRAM:Interferometer.

Software: MIR, MIRIAD, GILDAS, AIPS, MATLAB.

ORCID iDs

Geoffrey C. Bower https://orcid.org/0000-0003-4056-9982
Ramprasad Rao https://orcid.org/0000-0002-1407-7944
Natasha Maddox https://orcid.org/0000-0001-8312-5260
Elizabeth A. K. Adams https://orcid.org/0000-0002-9798-5111
C. J. Law https://orcid.org/0000-0002-4119-9963
Shriharsh P. Tendulkar https://orcid.org/0000-0003-2548-2926
Zsolt Paragi https://orcid.org/0000-0002-5195-335X
Shami Chatterjee https://orcid.org/0000-0002-2878-1502

References

Amorín, R., Muñoz-Tuñón, C., Aguerri, J. A. L., & Planesas, P. 2016, A&A, 588, A23
Bassa, C. G., Tendulkar, S. P., Adams, E. A. K., et al. 2017, ApJL, 843, L8
Bolatto, A. D., Wolfire, M., & Leroy, A. K. 2013, ARA&A, 51, 207
Cai, Y.-F., Sabancilar, E., Steer, D. A., & Vachaspati, T. 2012, PhRvD, 86, 043521
Chatterjee, S., Law, C. J., Wharton, R. S., et al. 2017, Natur, 541, 58
Cicone, C., Maiolino, R., Sturm, E., et al. 2014, A&A, 562, A21
Connor, L., Sievers, J., & Pen, U.-L. 2016, MNRAS, 458, L19
Davis, T. A., Bureau, M., Cappellari, M., Sarzi, M., & Blitz, L. 2013, Natur, 494, 328
de Zotti, G., Massardi, M., Negrello, M., & Wall, J. 2010, A&ARv, 18, 1
Domínguez, A., Siana, B., Henry, A. L., et al. 2013, ApJ, 763, 145
Dufour, R. J., Shields, G. A., & Talbot, R. J., Jr. 1982, ApJ, 252, 461
Falcke, H., & Rezzolla, L. 2014, A&A, 562, A137
Gajjar, V., Siemion, A. P. V., Price, D. C., et al. 2018, ApJ, in press (arXiv:1804.04101)
Gildas Team 2013, GILDAS: Grenoble Image and Line Data Analysis Software, Astrophysics Source Code Library, ascl:1305.010
Greisen, E. W. 2003, in Astrophysics and Space Science Library, Vol. 285, ed. A. Heck (Dordrecht: Kluwer), 109
Hatsukade, B., Ohta, K., Endo, A., et al. 2014, Natur, 510, 247
Kashiyama, K., & Murase, K. 2017, ApJL, 839, L3
Kobulnicky, H. A., & Kewley, L. J. 2004, ApJ, 617, 240
Kokubo, M., Mitsuda, K., Sugai, H., et al. 2017, ApJ, 844, 95
Law, C. J., Abruzzo, M. W., Bassa, C. G., et al. 2017, ApJ, 850, 76
Law, C. J., Bower, G. C., Burke-Spolaor, S., et al. 2015, ApJ, 807, 16
Leroy, A. K., Bolatto, A., Gordon, K., et al. 2011, ApJ, 737, 12
Leroy, A. K., Walter, F., Brinks, E., et al. 2008, AJ, 136, 2782
Loeb, A., Shvartzvald, Y., & Maoz, D. 2014, MNRAS, 439, L46
Lorimer, D. R., Bailes, M., McLaughlin, M. A., Narkevic, D. J., & Crawford, F. 2007, Sci, 318, 777
Lyutikov, M., Burzawa, L., & Popov, S. B. 2016, MNRAS, 462, 941
Marcote, B., Paragi, Z., Hessels, J. W. T., et al. 2017, ApJL, 834, L8
Metzger, B. D., Berger, E., & Margalit, B. 2017, ApJ, 841, 14
Ofek, E. O. 2017, ApJ, 846, 44
Oh, S.-H., Hunter, D. A., Brinks, E., et al. 2015, AJ, 149, 180
Perley, D. A., Niino, Y., Tanvir, N. R., Vergani, S. D., & Fynbo, J. P. U. 2016, SSRv, 202, 111
Petroff, E., Barr, E. D., Jameson, A., et al. 2016, PASA, 33, e045
Petroff, E., Johnston, S., Keane, E. F., et al. 2015, MNRAS, 454, 457

Reines, A. E., Greene, J. E., & Geha, M. 2013, ApJ, 775, 116
Reines, A. E., Sivakoff, G. R., Johnson, K. E., & Brogan, C. L. 2011, Natur, 470, 66
Rubio, M., Elmegreen, B. G., Hunter, D. A., et al. 2015, Natur, 525, 218
Sault, R. J., Teuben, P. J., & Wright, M. C. H. 1995, in ASP Conf. Ser. 77: Astronomical Data Analysis Software and Systems IV, Vol. 4, ed. R. A. Shaw, H. E. Payne, & J. J. E. Hayes (San Francisco, CA: ASP), 433
Schruba, A., Leroy, A. K., Walter, F., et al. 2012, AJ, 143, 138
Spitler, L. G., Cordes, J. M., Hessels, J. W. T., et al. 2014, ApJ, 790, 101
Tendulkar, S. P., Bassa, C. G., Cordes, J. M., et al. 2017, ApJL, 834, L7
Thornton, D., Stappers, B., Bailes, M., et al. 2013, Sci, 341, 53
Wilson, C. D., Warren, B. E., Israel, F. P., et al. 2012, MNRAS, 424, 3050
Wolfire, M. G., Hollenbach, D., & McKee, C. F. 2010, ApJ, 716, 1191